JOURNAL OF MATERIALS SCIENCE 23 (1988) 3951–3957

Determination of the flux pinning force of α-Ti ribbons in Nb46.5 wt % Ti produced by heat treatments of varying temperature, duration and frequency

P. J. LEE, D. C. LARBALESTIER*
*Applied Superconductivity Center and *Department of Metallurgical and Mineral Engineering, University of Wisconsin-Madison, Madison, Wisconsin 53706, USA*

Transmission electron microscopy has been used to investigate the effect of varying the heat treatment temperature, the duration and the frequency on the microstructure of high current density Nb–Ti superconducting composites. It was found that multiple heat treatment and drawing cycles produced between 16 and 25 vol % of α-Ti precipitate. The longer and more frequent were the heat treatments, the greater was the volume fraction of precipitate. An increase in the number of heat treatment and drawing cycles significantly reduced the size of the precipitates formed at heat treatment size. If the composites were drawn to final wire size following final heat treatment, the α-Ti precipitates were distorted into folded sheets which appeared as ribbons in transverse cross-section, with average thickness varying from 1.6 nm to 2.6 nm. The specific flux pinning force of the ribbons varied from 360 to 260 N m^{-2} and was found to decrease with ribbon thickness. Some evidence of an extrinsic limit on the J_c was provided by a study of the filament cross-section variability and the resistive transition index.

1. Introduction

In recent years there has been considerable progress in understanding the microstructures of superconducting Nb–Ti composites. Titanium-rich precipitates are first nucleated in the grain boundaries during initial heat treatment at 375–420° C, further heat treatment producing α-Ti precipitates typically 100–200 nm in diameter [1, 2]. These can be drawn out into a high density of ribbons only 1–2 nm thick, the transport J_c peaking for ribbons of this thickness [3]. In this latter work, we noted that the J_c peaked for ribbons much smaller than a coherence length (ξ) in thickness. The pinning of the fluxoid core in such a situation has been treated by Kramer and Freyhardt [4] and by Matsushita [5]. So far the balance of the evidence seems to show that the proximity effect does exist [7] but that it does not diminish the elementary pinning force [8], in the drastic fashion proposed by Kramer and Freyhardt.

The present study had several motivations. We wished to extend our earlier study of just one heat treatment process (six treatments of 10 h at 405° C) to a series of heat treatments. We wanted to see whether the volume of (normal) α-Ti precipitate depended significantly on processing or whether it was limited to the value of around 20% obtained previously [3]. By varying the number of heat treatments from three to six, we also hoped to discover whether the precipitate thickness–drawing strain relationships varied from heat treatment to heat treatment. However, we restricted this first part of the study to two heat treatments only (40 and 80 h at 420° C) in order to reduce the experimental variables somewhat. We have previously shown that these treatments are close to optimum for Nb46.5 wt % Ti [8].

A final important feature of these new experiments was the decision to use a niobium diffusion barrier clad composite. This avoids the problem of filament sausaging produced by Cu–Nb–Ti intermetallic and should, therefore, lead to better quality filaments with better n values. The measured transport J_c should then be closer to the intrinsic limits of the microstructure [9, 10]. However, this expectation was only partially fulfilled, as we discuss later.

2. Experimental design

2.1. Composite design and manufacture

A 55 filament single stack of niobium diffusion barrier clad NbTi sheathed in OFHC copper was fabricated by Oxford Superconducting Technology (OST). The NbTi alloy was of "High Homogeneity" grade supplied by Teledyne S. C. Company and was of nominal 46.5 wt % composition. The single stack was supplied to us at a diameter of 1.7 cm with a prior true strain of 5.6. Further processing and heat treatment was performed in our laboratory according to the schedules illustrated in Fig. 1a–d. It can be seen from the figure that two of the composites were processed directly as 55 filament conductors (CB4817/CB4837). However, there was insufficient strain space within which to give more than three heat treatments in a single stack. The majority of the composites were therefore processed

0022–2461/88 $03.00 + .12

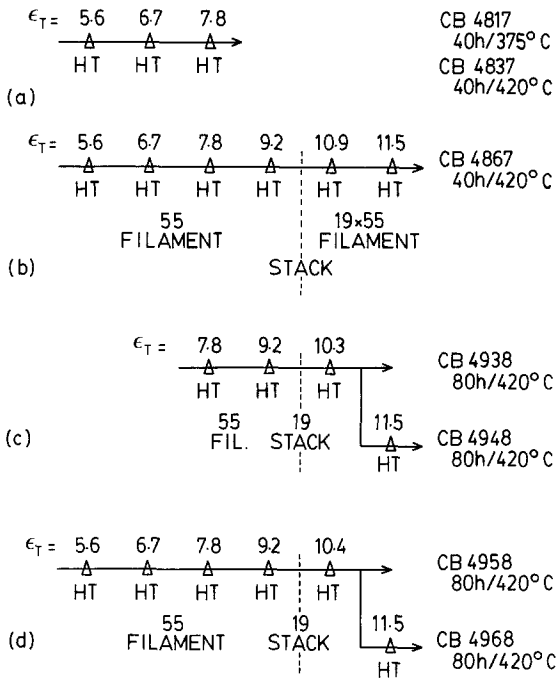

Figure 1 Heat treatment and drawing schedules (ε_T = nominal true drawing strain) for composites (a) CB4817 and CB4837, (b) CB4867, (c) CB4938 and (d) CB4958 and CB4968.

as a double stack (19 × 55), in order to provide sufficient strain space for up to six heat treatments.

2.2. Transmission electron microscopy

Wire samples were plated with copper until their diameter was 3 mm. 3 mm discs were cut in transverse cross-section and then ground to 100 μm thickness. The discs were thinned to perforation by jet electropolishing with a solution of 2 vol% HF, 5 vol% H_2SO_4 and 93 vol% methanol at $-40°$ C and with a polishing current density of 1.8 mA mm^{-2}. The transmission electron microscopy was performed on a JEOL 200CX TEM/STEM at 200 kV.

Quantitative measurements of precipitate transverse cross-sectional area were made at final heat treatment size on 20 × 25 cm^2 enlargements of the microstructure having a total magnification of 90 000. Areas were measured using a direct reading Numonics digitizer having a resolution of $\pm$0.25 mm. A minimum of 50 precipitates were measured for each heat treatment. α-Ti ribbon lengths and thicknesses were measured on composites CB4938, CB4948, CB4958 and CB4968 for wires with the highest J_c for each series. Measurements were made on 20 × 25 cm enlargements of transverse cross-sections with a total magnification of 600 000. A minimum of 50 ribbons for thickness measurement were selected by linear intercept, the minimum thickness at the point of intersection being measured. At least three randomly oriented lines were normally required to select the required number of ribbons. Line lengths were measured with a calibrated wheel having a resolution of 0.5 mm. Typical ribbon lengths per micrograph were 7–10 m.

2.3. Superconducting critical current measurements

Critical current (I_c) measurements were performed on ~0.6 m long samples mounted on copper and stainless steel barrels mounted coaxially inside the bore of a 12 T solenoid. The current was determined at an overall composite resistivity of 10^{-14} Ωm ($\approx 10\,\mu$V m^{-1}). The critical current density (J_c) was obtained from I_c using Cu : NbTi ratios obtained by weighing wire samples before and after nitric acid removal of the copper matrix. The resistive transition index, n, was determined from the slope of the log voltage–log current plot in the resistive transition, data being taken over the electric field range of about 10–40 μV m^{-1}.

3. Results

3.1. Final heat treatment microstructures

The heat treatments produced a two phase microstructure of β-NbTi and α-Ti. The majority of the α-Ti precipitates were formed at grain boundary triple points, these then growing out to a size comparable to the β-NbTi grains. Additional precipitate occurred as a thin titanium-rich film along grain boundaries of the β-NbTi matrix. The precipitates represented between 16 and 25% of the volume after final heat treatment. These precipitates were roughly equiaxed in transverse cross-section and were rather uniform in size and distribution. In the case of the composites heat treated for 80 h at 420° C, there was a tendency for precipitates to coalesce (Figs 2d–f). The more heat treatments that were given, the greater was the likelihood of this occurring. After three heat treatments (CB4938) (Fig. 2c), approximately 50% of the precipitates shared a surface with another precipitate, and after six heat treatments (CB4968), approximately 60% (Fig. 2f). For measurement purposes, the precipitates were treated as individual rather than coalesced particles. The measurements are given in Table I. In the case of CB4968 (6HT), measuring the adjoining precipitates as combined units would have increased the average precipitate cross-sectional area by 27%. The equivalent round diameter, D^*, was calculated from the measured cross-sectional area by assuming the precipitates to be of circular transverse cross-section.

The precipitate size and volume percentage grew

TABLE I Final heat treatment microstructure measurements

Wire designation	CB4817	CB4837	CB4867	CB4938	CB4948	CB4958	CB4968
Number of heat treatments	3	3	6	3	4	5	6
Heat treatment (h/° C)	40/375	40/420	40/420	80/420	80/420	80/420	80/420
Drawing strain at last HT	7.8	7.8	11.5	10.3	11.5	10.4	11.5
Volume % α-Ti after last HT	17	16	20	20	22	21	25
Average precipitate area (nm^2)	17 800	19 700	7 000	29 800	18 400	19 800	16 600
Equivalent round precipitate diameter (D^*) (nm)	151	158	94	195	153	159	145

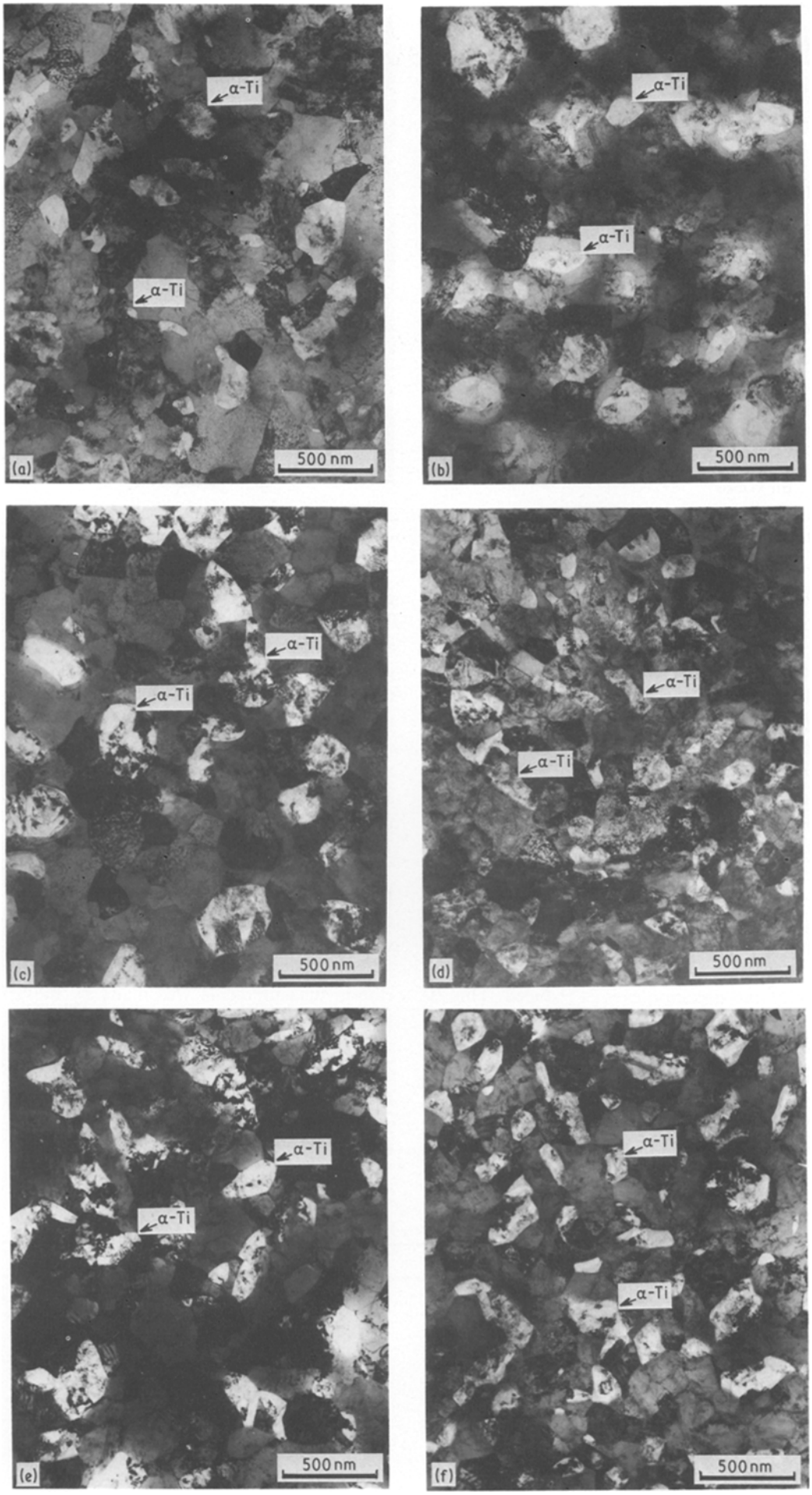

Figure 2 Transmission electron micrographs of filament cross-sections at final heat treatment size for (a) CB4817 (3HT of 40 h at 375° C), (b) CB4837 (3HT of 40 h at 420° C), (c) CB4938 (3HT of 80 h at 420° C), (d) CB4948 (4HT of 80 h at 420° C), (e) CB4958 (5HT of 80 h at 420° C) and (f) CB4968 (6HT of 80 h at 420°). All cross-sections are transverse, 3–5° from $\beta(110)$ drawing axis.

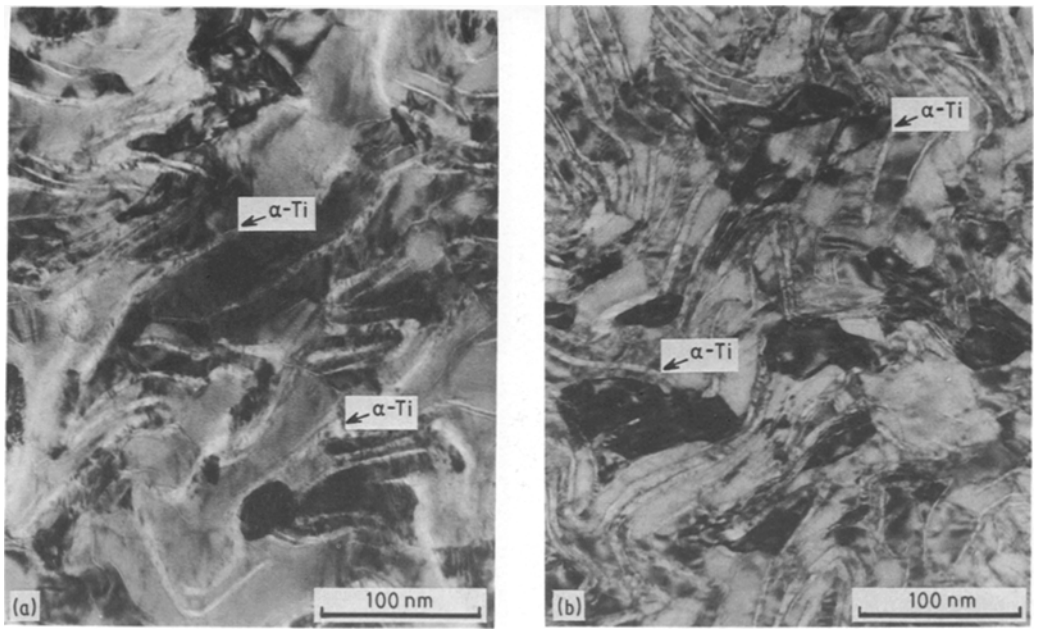

Figure 3 Transmission electron micrographs of filament cross-sections at 0.912 mm wire diameter for (a) CB4938 (3HT of 80 h at 420° C) and (b) CB4958 (5HT of 80 h at 420° C). Both cross-sections are transverse, 0.5–1.5° from $\beta(110)$ drawing axis.

slowly as the heat treatment time and temperature increased. For example, the results of increasing the time and temperature of three heat treatments, CB4817 (40 h 375° C), CB4837 (40 h 420°C) and CB4938 (80 h 420° C) (Figs 2a, b and c respectively), shows that %α increased from 17 to 20% and the average diameter from 151 to 195 nm. Increasing the heat treatment temperature from 375° C to 420° C (CB4817 and CB4837), while maintaining the time at 40 h, had little measurable effect on D^* or the volume fraction of precipitate. Doubling the heat treatment time from 40 to 80 h at 420° C (CB4837 and CB4938) was more significant. D^* increased by 23% and the volume percentage of α-Ti by approximately 25%.

The volume percentage of α-Ti increased with increasing number of 80 h/420° C heat treatments but the size of the precipitates was reduced. This is illustrated by comparing CB4938 (3HT), CB4948 (4HT), CB4958 (5HT) and CB4968 (6HT) (Figs 2c–f respectively). There was a 25% decline in D^* (195 nm to 145 nm) when increasing the number of heat treatments from 3 to 6, and a 25% increase in volume of precipitate (20% to 25%).

3.2. Final wire microstructures

The final wire transverse microstructures consisted of a rather homogeneous array of folded α-Ti ribbons with an average thickness ranging from 1.5 nm in CB4958 (Fig. 3a) to 2.6 nm in CB4938 (Fig. 3b). In this study only the wires with the maximum J_c (5 T) were measured. A comparison of Figs 3a and b reveals a substantial difference in ribbon spacing, this having an average value of 12.9 nm for the optimum CB4938 wire, and a value of 7.8 nm for the best CB4958 wire. The microstructural measurements are summarized in Table II. In all cases the majority of precipitates were less than 1.5 nm in thickness. In the case of CB4938, which had the thickest precipitates, 84% of the ribbons were less than 5 nm in thickness.

An independent check of the validity of these ribbon measurements was made by multiplying the total length of ribbon per unit area by the average measured thickness. This parameter (%α*) is given in Table II. It can be compared to the values of %α measured at heat treatment size, already presented in Table I. In all cases α* was less than α, as might be expected from the difficulty of detecting ribbons of less

TABLE II Final wire microstructure and superconducting property measurements

Wire designation	CB4938	CB4948	CB4958	CB4968
Number of heat treatments	3	4	5	6
Wire diameter (mm)	0.912	0.572	0.912	0.643
Filament diameter (μm)	16.2	10.1	15.8	11.2
Final drawing strain	4.41	4.18	4.41	3.95
Average ribbon thickness (nm)	2.6	2.2	1.5	1.6
Average ribbon separation (nm)	12.9	11.3	7.8	8.9
Ribbon length ($Mm\,m^{-2}$)	86.1	99.9	123	104
Measured %α (%α*)	17	16	17	16
(%α*/%α) %	85	73	81	64
J_c (5 T, 4.2 K) ($A\,mm^{-2}$)	3056	3029	3150	3062
n-value (5 T, 4.2 K)	54	35	48	45
$F_p$max (5 T, 4.2 K) ($GN\,m^{-2}$)	15.3	15.1	15.8	15.3
Q_{ppt} (5 T) ($N\,m^{-2}$)	356	302	257	294

than 1 nm thickness. Indeed the possibility exists that some α-Ti ribbons had been deformed to the point that they were no longer discrete α-Ti precipitates. The ratio α^*/α ranged from 0.85 to 0.64, declining with declining ribbon thickness, as expected by the above analysis.

3.3. Superconducting property results

The J_c (5 T) and J_c (8 T) values obtained as a function of final drawing strain are shown in Fig. 4 and the maximum values are summarized in Table II, along with the microstructural measurements. The curves of J_c plotted against ε is typical of those observed for Nb46.5 wt % Ti, J_c rising to a peak at a strain of about 4.5. What is more surprising is their lack of dependence on processing, J_c (5 T) at optimum strain varying only from ~ 2900 to 3150 A mm^{-2}. This result was found whether 3, 4, 5 or 6 heat treatments were used. Resistive transition index values (n) are indicated next to the J_c points in the figure. They ranged from about 70 to 30, being generally larger for smaller strains and a smaller number of heat treatments.

4. Discussion

The particular goals of this work were to extend our previous microstructural studies [1–3] on composites heat treated at lower temperatures (e.g. 375 or 405° C) or for shorter periods (e.g. 10 h) to more optimum values and to extend the number of heat treatments beyond the 2 and 3 which had previously received an extensive J_c investigation, [9]. We also wished to minimize filament instabilities [11] by utilizing a composite clad with niobium which would prevent intermetallic nodule growth [12, 13]. The 55 filament design of sub-element used in the present study has been used by Hong to develop 3700 A mm^{-2} at 5 T, using variants of the heat treatment previously described [9].

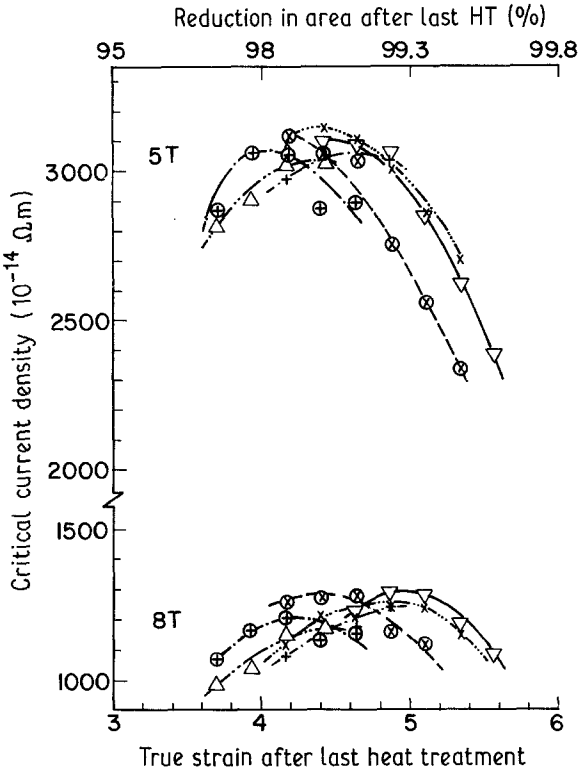

Figure 4 Variation in critical current density (4.2 K, 10^{-14} Ωm) with final drawing strain and area reduction. (——▽—— CB4857, ——⊗—— CB4867, -·-·-+-·-·- CB4938, —·—▲—·— CB4948, —·—·—x—·—·— CB4958, —·—⊕—·— CB4968).

The microstructual information obtained in this study considerably extends that previously published [1–3]. On our recent study [3], we presented quantitative information linking the J_c to the optimized ribbon precipitate morphology. In that study we found that α-Ti nucleated as a film in the grain boundaries, growing out to approximately equiaxed (in transverse cross-section) precipitates of about 90 nm in diameter after 6HT of 10 h at 405° C. Drawing this composite after heat treatment caused J_c (5 T) to peak at a final drawing strain of about 3.3, the mean α-Ti ribbon thickness then being 1 nm. Analysis of the resistive transition showed that the intrinsic J_c (i.e. that determined by the flux pinning in the microstructure rather than by filament sausaging) was peaking for even smaller precipitates, though the location of the peak was not determined.

The present study confirms the general features of the previous study in respect of the mode of formation of the α-Ti and the effect of drawing (Figs 2 and 3). The quantitative microstructural parameters are different, however. The longer, higher temperature heat treatments (Table I) produced significantly larger α-Ti precipitates (94–195 nm) than those previously observed [3] for 10 h at 405° C (87 nm). This is not an unexpected result. The volume of precipitate after the final heat treatment is also generally larger (16–25%), as compared to 17% in the prior study. The optimum final drawing strain is also higher in the present experiments, being 4 to 4.4, as compared to 3.3 in the earlier experiments. We believe that this is a consequence of the protective effect of the niobium diffusion barrier.

In a recent extensive study of the effects of two and three heat treatments on the J_c, Li and Larbalestier [8], showed that the slope of the J_c–ε_f plot was constant over a significant strain range (~ 2 to 5) and showed a systematic increase as the heat treatment temperature was raised from 375 to 435° C and as the heat treatment (HT) time was lengthened. Although no microstructural examinations were performed in that study, it was concluded that such regular behaviour must have its origin in systematic rearrangements of the α-Ti flux pinning centres of the type observed here.

An approach to making our microstuctural observations of quantitative use for flux pinning studies can be derived from a calculation of the specific pinning force (Q), defined as

$$Q = F_p/\lambda S$$

where F_p is the bulk pinning force ($J_c \times B$), S is the dimensional parameter of the pinning centre (the area of precipitate per unit volume in this case) and λ a pinning efficiency factor. λ is not well known; we use the value of $\frac{1}{2}$ previously used for columnar grains [1, 14, 15], which also appears appropriate for long laminar precipitates.

The values of Q_{ppt} obtained in the previous study [3] ranged from 260 to 170 N m^{-2}, declining as the precipitates became thinner. In the present study the precipitates are a little thicker and the values of Q_{ppt} are somewhat larger (260–360 N m^{-2}), thus showing a

similar correlation with precipitate thickness. It seems clear, that the elementary pinning force of the precipitates does decline slowly as their thickness is reduced from about 2.5 nm to less than 1 nm. However the effect is only of order 2, rather than the very much larger effects previously predicted [4]. We have recently shown [6] that a significant proximity effect depression of the T_c does arise as the precipitates are drawn from their heat treatment size to the optimum size. Thus Matsushita's view of the proximity effect on the elementary pinning force (f_p) is supported [5]. However, even though f_p (or its measured value Q_{ppt}) declines slightly during drawing, the total pinning force (F_p) continues to increase, since the density of interactions increases. A more detailed study of these effects by Meingast *et al.* [8] is currently nearing completion.

A final caution concerning these results is appropriate. We have elsewhere emphasized the need to identify extrinsic factors which produce a limit on the transport J_c below that of the intrinsic microstructure–flux lattice interaction [16]. In spite of the supression of intermetallics by the niobium diffusion barrier, the n value data gives clear evidence of filament sausaging. This filament irregularity reduced the ratio I_c (measured)/I_c (average) [10, 17] and leads to an underestimate of the intrinsic J_c. Partial quantification of this effect is given in Fig. 5 and Table III. Fig. 5 presents histograms of filament cross-sectional areas (CSA) for the central 55 filament bundle in the 19 × 55 filament stacks of CB4938 (3HT) and CB4968 (6HT). The distribution is considerably less sharp for the composite with 6HT ($\sigma_{n-1}/\bar{A}$ is 12.4% as opposed to 8.8%). The perturbation is particularly large for the outer ring of filaments (17.1% and 12.1% for 6 and 3HT composites respectively). These numbers demonstrate the detrimental effect of the additional heat treatments rather clearly. These numbers, being taken from the centre 55 filament bundle, may well underestimate the total problem, since the outer filament bundles tend to show a little more damage than the inner ones.

TABLE III Filament uniformity cross-sectional areas of centre bundle filaments

	CB4938 0.912 mm diameter $\varepsilon_f = 4.41$	CB4968 0.643 mm diameter $\varepsilon_f = 3.94$
σ_{n-1} (% CSA) Row 1 outer (18 filaments)	12.1	17.1
σ_{n-1} (% CSA) Row 2 (18 filaments)	5.9	11.0
σ_{n-1} (% CSA) Rows 3, 4 and 5 (19 filaments)	7.7	7.5
σ_{n-1} (% CSA) All filaments (55 filaments)	8.8	12.4
% of filaments deviating from mean CSA by > 5%	41.8	72.7
% of filaments deviating from mean CSA by > 10%	21.8	30.9

At this stage we do not understand all the factors leading to filament instability. One important parameter has recently been reported to be the filament separation (s) to filament diameter (d) ratio, s/d ratios of less than 0.2 being proposed as optimum [18]. The s/d ratio of this composite is variable, there being substantial copper between the 55 filament subbundles. Thus the outer ring filament instability may be provoked by a high local s/d ratio. Since the s/d ratio is really a parameter which measures the mechanical support given to the filaments by the matrix, it is not surprising that increasing the number of heat treatments (which act as recrystallization anneals for the copper) also increases the filament irregularity.

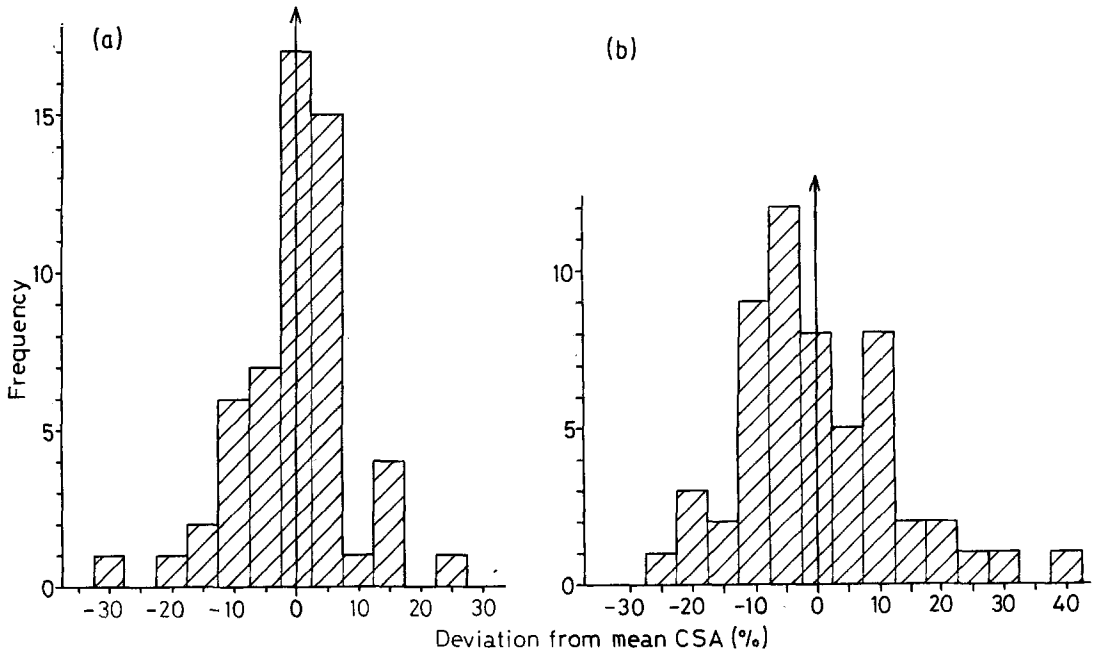

Figure 5 Distribution of filament cross-sectional areas (CSA) for the central filament bundle (55 filaments) for (a) CB4938 (3HT of 80 h at 420° C) at 0.912 m wire diameter and (b) CB4968 (6HT of 80 h at 420° C) at 0.643 mm diameter.

Further evidence for the crucial role of filament instability in limiting J_c can be obtained by comparing the present results on CB4938 to those of Li and Larbalestier [9] on a monofilament conductor given the same heat treatment of 3 times 80 h at 420° C. Both composites had $J_c(5\,T) = 3050 \pm 50\,A\,mm^{-2}$ at $\varepsilon_f = 4.4$. However, J_c (5 T) peaks at $\varepsilon_f = 4.4$ for the multifilament CB4938 of the present study, while J_c was still increasing for the monofilament conductor at the highest strain tested, reaching $3700\,A\,mm^{-2}$ at $\varepsilon_f = 5.2$. The complete radial symmetry and small copper to superconductor ratio of the monofilament conductor is evidently helpful in maintaining filament quality to extraordinarily high strains. It thus seems appropriate to say that the values of Q_{ppt} reported here are lower limits. The intrinsic values of Q_{ppt} and J_c should be somewhat higher than the experimental values reported here [19, 20, 21] and further analysis is needed to clarify these points.

5. Conclusions

(1) Up to 25 vol % of α-Ti was produced by multiple heat treatments.

(2) The longer and more frequent the heat treatments, the greater was the volume percentage of precipitate.

(3) The precipitate size produced after final heat treatment decreased with increasing number of heat treatment and drawing cycles.

(4) The average α-Ti ribbon thickness for the optimized wires ranged from 1.6 nm to 2.6 nm, significantly less than the coherence length, (~ 5 nm), and the fluxoid diameter (~ 10 nm).

(5) As the ribbon thickness decreased the specific ribbon pinning force decreased varying from 360 to $260\,N\,m^{-2}$.

Acknowledgements

We are grateful to C. Meingast and W. Warnes for helpful discussions and to S. Hong (Oxford Superconducting Technology) for supply of the 55 filament rod stock. W. Starch rendered valuable experimental assistance. The continued collaboration of R. M. Scanlan (Lawrence Berkeley Laboratory) is greatly appreciated. The work has been supported by the Department of Energy-Division of High Energy Physics.

References

1. D. C. LARBALESTIER and A. W. WEST, *Acta Metall.* **32** (1984) 1871.
2. A. W. WEST and D. C. LARBALESTIER, *Met. Trans. A* **15** (1984) 843.
3. P. J. LEE and D. C. LARBALESTIER, *Acta Metall.* **35** (1987) 2523.
4. E. J. KRAMER and H. C. FREYHARDT, *J. Appl. Phys.* **51** (1980) 4930.
5. T. MATSUSHITA, *ibid.* **54** (1983) 281.
6. C. MEINGAST, M. DAEUMLING, P. J. LEE and D. C. LARBALESTIER, *Appl. Phys. Lett.* **51(9)** (1987) 688.
7. E. W. COLLINGS, T. S. KREILICK, E. GREGORY, P. J. LEE and J. C. HO, *Adv. Cryogenic Engng* **34** (1988) 1027.
8. C. MEINGAST, P. J. LEE and D. C. LARBALESTIER, To appear.
9. LI CHENGREN and D. C. LARBALESTIER, *Cryogenics* **27** (1987) 171.
10. W. H. WARNES and D. C. LARBALESTIER, *ibid.* **26** (1986) 643.
11. *Idem., Appl. Phys. Lett.* **48** (1986) 1403.
12. K. HEMACHALAM, C. G. KING, B. A. ZEITLIN and R. M. SCANLAN, *Adv. Cryogenic Engng* **32** (1986) 731.
13. D. C. LARBALESTIER, P. J. LEE and R. W. SAMUEL, *ibid.* **32** (1986) 715.
14. E. J. KRAMER, *ibid.* **28** (1982) 307.
15. W. YETTER and E. J. KRAMER, *J. Mater. Sci.* **17** (1982) 2792.
16. D. C. LARBALESTIER, *IEEE Trans. Magnetics* **21** (1985) 257.
17. C. PLUMMER and J. E. EVETTS, *IEEE Trans. MAG.* **23** (1987).
18. E. GREGORY, T. S. KREILICK, J. WONG, A. GHOSH and W. B. SAMPSON, *Cryogenics* **27** (1987) 178.
19. W. H. WARNES and D. C. LARBALESTIER, *IEEE Trans. MAG.* **23** (1987).
20. W. H. WARNES, *Adv. Cryogenic Engng* submitted.
21. L. COOLEY, W. H. WARNES and D. C. LARBALESTIER, *Adv. Cryogenic Engng.* submitted.

Received 27 October 1987
and accepted 25 February 1988